Environmental Science Nano

ROYAL SOCIETY OF CHEMISTRY

PAPER

View Article Online
View Journal | View Issue

Cite this: *Environ. Sci.: Nano*, 2024, 11, 578

Delineating the role of surface grafting density of organic coatings on the colloidal stability, transport, and sorbent behavior of engineered nanoparticles†

Junseok Lee,[a] Changwoo Kim,[b] Daniel Schmucker,[c] Seung Soo Steve Lee,[a] Shuchi Liao,[d] Natalie L. Cápiro,[e] Kurt D. Pennell[d] and John D. Fortner*[a]

Received 2nd June 2023,
Accepted 11th August 2023

DOI: 10.1039/d3en00358b

rsc.li/es-nano

Aqueous stability and sorption affinity (towards target environmental contaminants) of engineered nanoparticles, composed of inorganic nanoparticles and surface stabilizers, underpin their environmental behavior and application potential for a variety of proposed technologies. However, fundamentally delineating the role of surface coatings (in terms of surface coating density) remains outstanding for a number of particle systems. To address this critical issue, we describe colloidal stability, transport, and sorption behavior of engineered manganese oxide nanoparticles as a function of specific surface grafting density. We observed higher grafting density results in higher colloidal stability due to higher steric repulsion forces. Additionally, humic acid (HA) significantly improved the stability of NPs with lower grafting density, while showing negligible effects in higher grafting density. Deposition behavior did not correlate with grafting density, regardless of organic coating types. In the presence of HA, deposition behavior of negatively charged NPs was not altered, while deposition of positively charged NPs was dependent on HA presence. Higher grafting density of CTAB also enhanced chromate sorption capacity due to the increasing number of favorable functional groups. Taken together, this work clearly demonstrates the critical need to fully understand NP surface coating dynamics as they relate to fundamental material behavior and performance.

Environmental significance

Nanoparticle behavior in water is governed by surface properties, including effective surface-based coatings. Here we quantitatively describe the critical role of surface coatings with regard to grafting density of the stabilizing organic layer (*i.e.* number of stabilizing agents per surface area), on the aggregation, transport, and sorption behavior of engineered nanoparticles. For these, we explore particle behavior in relevant water chemistries, including the role of natural organic matter.

Introduction

Modification of engineered nanoparticles (NPs) surfaces with organic surfactants has received considerable attention in recent years.[1–3] Surface functionalization of NPs not only enhances the physicochemical and mechanical properties, but also improves their biocompatibility.[4] For example, NP surface functionalization can improve colloidal stability of NPs in water,[5,6] preventing dissolution,[7] enhance reactivity/remediation of potentially harmful substances,[8,9] and even mitigate toxicity.[10] Additionally, as the production and applications of engineered NPs continues to increase, the corresponding potential for environmental exposure is also increased, furthering the need to fundamentally predict NP behavior.

Following intentional or accidental release of engineered NPs into the environment, their fate and transport are largely governed by particle–particle and particle–surface interactions, and thus, when present, surface (organic) NP coating plays a critical role. For instance, He *et al.* observed that zerovalent iron NPs coated with carboxymethyl cellulose exhibited enhanced

[a] *Department of Chemical and Environmental Engineering, Yale University, New Haven, CT, 06511 USA. E-mail: john.fortner@yale.edu; Tel: +1 314 935 9293*
[b] *School of Earth Sciences and Environmental Engineering, Gwangju Institute of Science and Technology, Gwangju 61005, Republic of Korea*
[c] *Department of Energy, Environmental and Chemical Engineering, Washington University in St. Louis, St. Louis, MO, 63130 USA*
[d] *School of Engineering, Brown University, Providence, RI, 02912 USA*
[e] *Department of Biological and Environmental Engineering, Cornell University, Ithaca, NY, 14853 USA*

† Electronic supplementary information (ESI) available. See DOI: https://doi.org/10.1039/d3en00358b

transport behavior in a simulated aquifer due to surface-based electrostatic stabilization (preventing the NPs aggregation and deposition).[11] Phenrat *et al.* showed that dispersion stability of zerovalent iron NPs was enhanced by surface modification *via* polyelecetrolytes when compared to 'bare' NPs.[12] Li *et al.* reported that silver NPs coated with Tween 80 were significantly more stable than uncoated silver NPs.[13] When considering specific surface coating properties, the grafting density of organic molecules on the surface is a crucial, yet often under studied (and under reported), factor governing the magnitude of both electrostatic and steric repulsion forces related to aggregation and deposition behavior(s).[14]

Organic coatings also affect the sorption behavior of engineered NPs *via* specific affinity between organic coated NPs and target contaminants. For example, Lee *et al.* demonstrated that phosphonic acid group on manganese ferrite NPs showed highest sorption capacity for uranium removal rather than positively charged surface coating.[15] Kim *et al.* showed that iron oxide NPs with positively charged surface coatings have higher sorption capacity for arsenic and chromium sorption compared to negatively charged NPs.[16] Huang and Keller revealed that magnetic NPs functionalized with EDTA showed high sorption capacity for heavy metal removal for a variety of water chemistries as well as material regeneration.[17] Among these and numerous other studies, it is clear that surface coating density is a critical NP design criterion,[18–20] yet remains relatively understudied.

While there are many reports on NP surface coatings,[21] direct evaluation of NP behavior(s) as a function of surface coating density has not been extensively investigated due to the required synthesis precision and associated (and incomparable) stability regimes. In this study, we examined NP behavior as a function of carefully controlled grafting densities, comparing colloidal stability, transport, and sorption behavior as well as exploring the effects of natural organic matter (NOM), as humic acid (HA). For this, we evaluated the effect of grafting density on colloidal stability in terms of critical coagulation concentration (CCC), as quantified *via* aggregation kinetics. Sand column tests were also performed and modeled to evaluate NP deposition behavior as a function of grafting density and coating type, along with the presence of HA. Lastly, sorption capacities for chromate (as an example inorganic pollutant) are demonstrated as a function of surface coating grafting density.

Methods

Materials

Manganese(II) chloride tetrahydrate ($MnCl_2{\cdot}4H_2O$, 99.99%), oleic acid (OA, 90%), 1-octadecene (90%), polyethyleneglycol (PEG, MW = 5000), cetyltrimethylammonium bromide (CTAB, 95%), hexane (98.5%), acetone (99.5%), ethanol (99.9%), sodium chloride (NaCl, 99%), calcium chloride ($CaCl_2$, 99%), nitric acid (HNO_3, 70%), sodium hydroxide (NaOH, 97%), sodium bicarbonate ($NaHCO_3$, 99.7%), potassium chloride (KCl, 99%), potassium bromide (KBr, 99.95%), potassium chromate ($K_2Cr_2O_7$, 99%), and humic acid (HA, technical grade) were purchased from Sigma-Aldrich. Sodium oleate (97%) was purchased from TCI America. Nitrogen gas (N_2, 99.999%, Airgas) was used to synthesize NPs.

Preparation of manganese oxide nanoparticles

Manganese oxide (Mn_xO_y) NPs were synthesized by thermal decomposition of manganese oleate as a Mn_xO_y precursor at 320 °C. Detailed procedures for synthesis of manganese oleate and Mn_xO_y NPs were reported in previous studies.[22,23] The synthesized NPs were purified over six times by centrifuging at 7000 rpm using acetone, ethanol, and hexane. The purified Mn_xO_y NPs were dispersed and stored in hexane. The resulting Mn_xO_y NPs were phase transferred using various surface stabilizing agents, such as OA, PEG, and CTAB (Mn_xO_y@OA, Mn_xO_y@PEG, and Mn_xO_y@CTAB). Different concentrations of stabilizing agent were mixed with 10 mL of ultrapure water (18.2 MΩ cm, Millipore) and 0.4 mL of Mn_xO_y NPs in hexane solution (2.2×10^{14} NPs per liter) through probe sonication (UP50H, Hielscher) at 80% amplitude and full cycle for 10 min. The resulting solution (in an opened vial) were stored under the fume hood to remove the remaining hexane in solution for 24 h, and subsequently the residual of surface stabilizers in the solution was removed by ultrafiltration membrane (cellulose, 100 kDa MWCO, Millipore) under stirring, followed by syringe filtration (0.22 μm PES, Millipore).

The grafting density on the NPs was determined using total organic carbon (TOC, TOC-L analyzer, Shimadzu Corporation) measurements. The number of organic molecules per NPs was quantified by difference of TOC values between the solution with the organic coated NPs and supernatant without the NPs removed by ultracentrifuge (Sorvall WX Ultra 80, Thermo Scientific) at 50 000 rpm for 2 h, with assumption of equivalent distribution for organic molecules to the NPs. The concentration of NPs was determined by digestion of NPs with hydrochloric acid (1 N) under heating (80 °C) and measuring their manganese concentration using inductively coupled plasma-optical emission spectrometer (ICP-OES).

Critical coagulation concentration (CCC)

Aggregation kinetic of NPs was evaluated by measuring hydrodynamic diameter (D_H) of Mn_xO_y NPs (*ca.* 1 mg L^{-1} as Mn concentration) with different grafting densities in the absence and presence of HA as a function of NaCl and $CaCl_2$ concentrations for 20 min. Their D_H was measured using a Malvern Nano ZS system by Malvern Panalytical (Malvern Zetasizer Nanoseries, Malvern, UK). All measurements were conducted at a room temperature of 22 °C. The solution pH was adjusted to 7.0 ± 0.2 with HNO_3 and NaOH solutions. The colloidal stability of NPs having different grafting densities was evaluated by comparing CCC values in which the aggregation kinetic reached to diffusion-limited regimes

(*i.e.*, the attachment efficiency is equal to 1). The attachment efficiency (α) for aggregated NPs was calculated by following equation:

$$\alpha = \frac{1}{W} = \frac{k}{k_{fast}} \quad (1)$$

where W is stability ratio, k is aggregation rate constant obtained at interested salt concentrations, and k_{fast} is diffusion-limited aggregation rate constant obtained under favorable aggregation conditions.[24,25]

Column experiments

Column experiments were performed in water saturated columns packed with 30–40 mesh Ottawa sand through a glass column (Spectra/Chrom, TX) with dimensions of 15 cm in length and 1.5 cm in inner diameter. Prior to transport tests, the packed column was flushed with DI water and desired background solution. Following water saturation, a nonreactive tracer (KBr) test was performed to assess hydrodynamic properties of the porous media, and the resulting porosity was determined to be *ca.* 0.39. All experiments were conducted at a pore-water velocity of 0.76 m d^{-1}, which is in the range of typical values of real groundwater flow.[26–28] For NPs transport experiments, a 5 pore volume (PV) pulse of solution containing Mn_xO_y NPs with different grafting densities (1 mg L^{-1} as Mn concentration) under same background electrolyte composition was introduced to the column, followed by the injection of a NP-free background solution. Column effluent samples were collected continuously using fraction collector and NP concentration was measured by ICP-OES as described above. Following each transport experiments, the columns were sectioned into 5 increments, and retained NPs concentrations were extracted and measured using ICP-OES to assess their spatial distribution in the column. Detailed information about the column experiment methods are provided in the ESI.†

The resulting data of column tests were interpreted using clean-bed filtration theory (CFT)[29] and a modified filtration theory (MFT) approach.[30] In CFT, the attachment efficiency (α) of NPs to the sand was calculated by the following equation:

$$\alpha = -\frac{2}{3}\frac{d_c}{(1-\varepsilon)L\eta_0}\ln\frac{C_e}{C_0} \quad (2)$$

where d_c is diameter of sand [L], ε is porosity of packed column, L is length of the column [L], η_0 is single collector efficiency, C_e is effluent concentration of NPs, and C_0 is influent concentration of NPs [M L^{-3}]. The single collector efficiency (η_0) was numerically estimated using the empirical equation:[31]

$$\eta_0 = 2.4A_S^{1/3}N_R^{-0.081}N_{Pe}^{-0.715}N_{vdW}^{0.052} + 0.55A_SN_R^{1.675}N_A^{0.125} + 0.22N_R^{-0.24}N_G^{1.11}N_{vdW}^{0.053} \quad (3)$$

where A_S is Happel model parameter, N_R is aspect ratio, N_{Pe} is Peclet number, N_{vdW} is van der Waals number, N_A is attraction number, and N_G is gravitational number. Each term in above equation represents the three filtration mechanisms; diffusion, interception, and sedimentation, respectively. In the MFT approach, a traditional mass balance equation that accounts advection, hydrodynamic dispersion and particle deposition was solved to simulate NP effluent concentration and solid phase retention profiles:

$$\frac{\partial C}{\partial t} + \frac{\rho_b}{\theta_w}\frac{\partial S}{\partial t} = D_h\frac{\partial^2 C}{\partial x^2} - v_p\frac{\partial C}{\partial x} \quad (4)$$

Here, C and S are the NP aqueous and solid-phase concentrations [M L^{-3} and M M^{-1}] respectively; t is time [t], x is the distance from the column inlet [L]; v_p is the average pore-water velocity [L t^{-1}], D_h is the hydrodynamic dispersion coefficient for the column [L^2 t^{-1}], ρ_b is the bulk density of the porous medium [M L^{-3}], and θ_w is the volumetric water content [L^3 L^{-3}].

For NP deposition, a Langmuir-type site block function was employed to describe the rate of attachment (k_{att}, 1/t) as attachment sites were occupied, and a first-order detachment term (k_{det}, 1/t) was included to account for nanoparticle release:[32]

$$\frac{\rho_b}{\theta_w}\frac{\partial S}{\partial t} = k_{att}\Psi C - \frac{\rho_b}{\theta_w}k_{det}S \quad (5)$$

$$\Psi = \frac{S_{max} - S}{S_{max}} \quad (6)$$

Here, S_{max} is the maximum capacity of the solid phase for NP deposition. eqn (4)–(6) were implemented to fit the NP effluent breakthrough curve (BTC) data using a central-in-space and fully implicit-in-time finite difference scheme in MATLAB R2022b (MathWorks, Natick, MA). The fitted parameters, including k_{att}, k_{det} and S_{max}, are listed in Table S2.† The NP retention profiles were then simulated using the fitted parameters.

Chromate sorption measurements

The phase transferred Mn_xO_y NPs with different grafting densities (20 mg L^{-1} as Mn concentration) were tested for chromate sorption (10 mg L^{-1} as Cr(VI)) at pH 7. Chromate sorption dynamics was proceeded for 24 h and the solution pH was adjusted to 7.0 ± 0.2 twice (initially and after 4 h during each batch sorption experiment) using HNO_3 and NaOH solutions. After mixing for 24 h (equilibrium), the NPs were separated using ultracentrifuge at 50 000 rpm for 2 h and remaining concentration of Cr(VI) in the supernatant was measured by ICP-OES. All experiments were performed in duplicate. The measured chromate sorption density (mass of adsorbed chromate per mass of Mn_xO_y NPs in the sample) was compared with respect to the grafting density of NPs.

Results and discussion

Characterization of manganese oxide nanoparticles with different grafting densities

Monodisperse manganese oxide (Mn_xO_y) NPs were synthesized through thermal decomposition of manganese oleate at 320 °C, resulting in highly crystalline NPs, stable in various nonpolar organic solvents such as, toluene and hexane (Fig. S1†). As reported in our previous work,[23] synthesized Mn_xO_y NPs are demonstrated to be a core shell structure (a core particles of MnO with a thin shell of Mn_3O_4 particles). We selected Mn_xO_y NPs due to our ability to precisely control particle shape and size during synthesis and for their antiferromagnetic property of core particle at room temperature, thus negating potential interfering magnetic effects.[33] Synthesized Mn_xO_y NPs (18.4 ± 1.5 nm) were then varied by carefully controlling concentrations of surface stabilizing agents added during the final phase transfer stepphase transferred into water *via* various surface coatings (*i.e.* stabilizing organic layer), including OA, CTAB, *via* ligand encapsulation method (Mn_xO_y@OA, Mn_xO_y@CTAB),[34–36] and PEG by ligand encapsulation (Mn_xO_y@PEG)[20] to render NPs hydrophilic and stable in aqueous media.

During the phase transfer process, the number of (surface) organic molecules per NPs (*i.e.*, grafting density) was precisely varied by carefully controlling concentrations of surface stabilizing agents added during the final phase transfer step. The D_H of those phase-transferred NPs with different grafting densities is presented in Fig. 1. For the same surface coating, the D_H was consistent regardless of the grafting density, which indicates that the organic molecules on the outer-most layer were similarly oriented (*e.g.* no additional layering). The average D_H of organic functionalized NPs was around 25 to 31 nm for MnO@OA, 36 to 48 nm for MnO@PEG, and 27 to 41 nm for MnO@CTAB, in a wide range of grafting density, respectively. As shown in Fig. 1, the bilayer coating structure with OA and CTAB showed relatively small D_H compared with PEG coating(s), which is in line with our previous studies.[16,23] Zeta potential measurements of surface functionalized Mn_xO_y NPs (Fig. S2†) were −36 to −34 mV for MnO@OA, −11 to −28 mV for MnO@PEG, and 16 to 41 mV for MnO@CTAB, which are also similar to our previous studies.[15,23,34]

Colloidal stability

Colloidal stability of the phase-transferred NPs was evaluated with respect to the grafting density by measuring CCC values as a function of NaCl and $CaCl_2$ concentrations. As shown in Fig. 2, water stable NPs with various grafting density, were evaluated in mono- or di-valent cationic salt solutions and their colloidal stability was monitored and compared. For these, the higher grafting density materials demonstrated higher stability, as larger CCC values were observed for both NaCl and $CaCl_2$ solutions (Fig. 2(a–d)). Specifically, CCC values for higher grafting density of Mn_xO_y@OA (855 mM of NaCl and 21.8 mM of $CaCl_2$) and Mn_xO_y@PEG (283 mM of NaCl and 8.5 mM of $CaCl_2$) were higher than those for lower grafting density of Mn_xO_y@OA (236 mM of NaCl and 11.2 mM of $CaCl_2$) and Mn_xO_y@PEG (173 mM of NaCl and 1.8 mM of $CaCl_2$), respectively. We hypothesize that, higher grafting densities lead to higher electrostatic and steric repulsion forces due to higher entropic restriction and osmotic pressure difference(s), and thus consequently resulted in higher colloidal stability.[37–39] It should be noted that aggregation kinetics for Mn_xO_y@CTAB were unfavorable under high NaCl (2000 mM) and $CaCl_2$ (1000 mM) concentrations and therefore, stability based on CCC values could not be compared (Fig. S3†).

As NOM is ubiquitous and can form complexes with metal oxides in natural water, we further investigated the colloidal stability of water stable NPs (with a varied grafting densities) in the presence of humic acid (HA). For these systems, HA in water actually improves the colloidal stability of NPs with low grafting density. In the presence of HA (1 mg L^{-1} TOC), phase-transferred NPs with low grafting density showed a significant increase in CCC value in NaCl compared to the absence of HA. For Mn_xO_y@OA, the CCC for lower grafting density in the presence of HA were 1325 mM of NaCl, which was substantially higher than 236 mM of NaCl in the absence of HA. In contrast, higher grafting density NPs had similar or slightly higher CCC value (994 and 855 mM of NaCl in the presence or absence of HA, respectively). Similar results were obtained for Mn_xO_y@PEG, where the CCC for lower grafting density showed dramatic increase from 173 to 1372 mM of NaCl in the presence of HA. As observed in previous studies, HA can improve

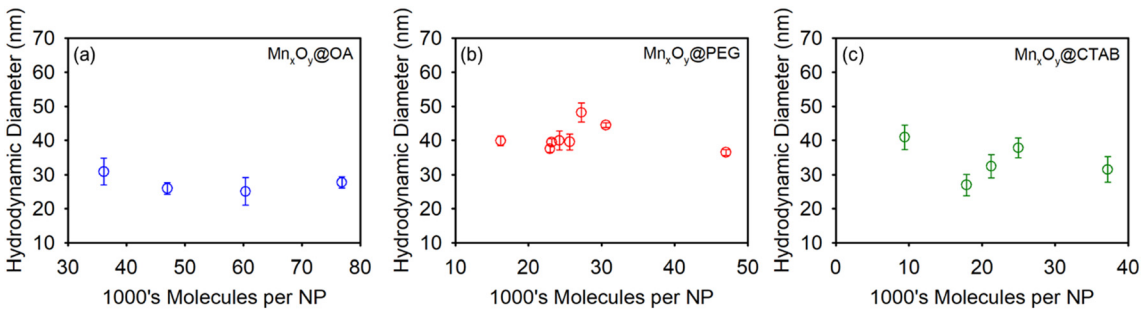

Fig. 1 Hydrodynamic diameter (D_H) of the surface functionalized manganese oxide nanoparticles (Mn_xO_y NPs) with different surface grafting densities at pH 7.0 ± 0.2. Mn_xO_y NPs coatings include OA, PEG, and CTAB, here as: (a) Mn_xO_y@OA, (b) Mn_xO_y@PEG, and (c) Mn_xO_y@CTAB.

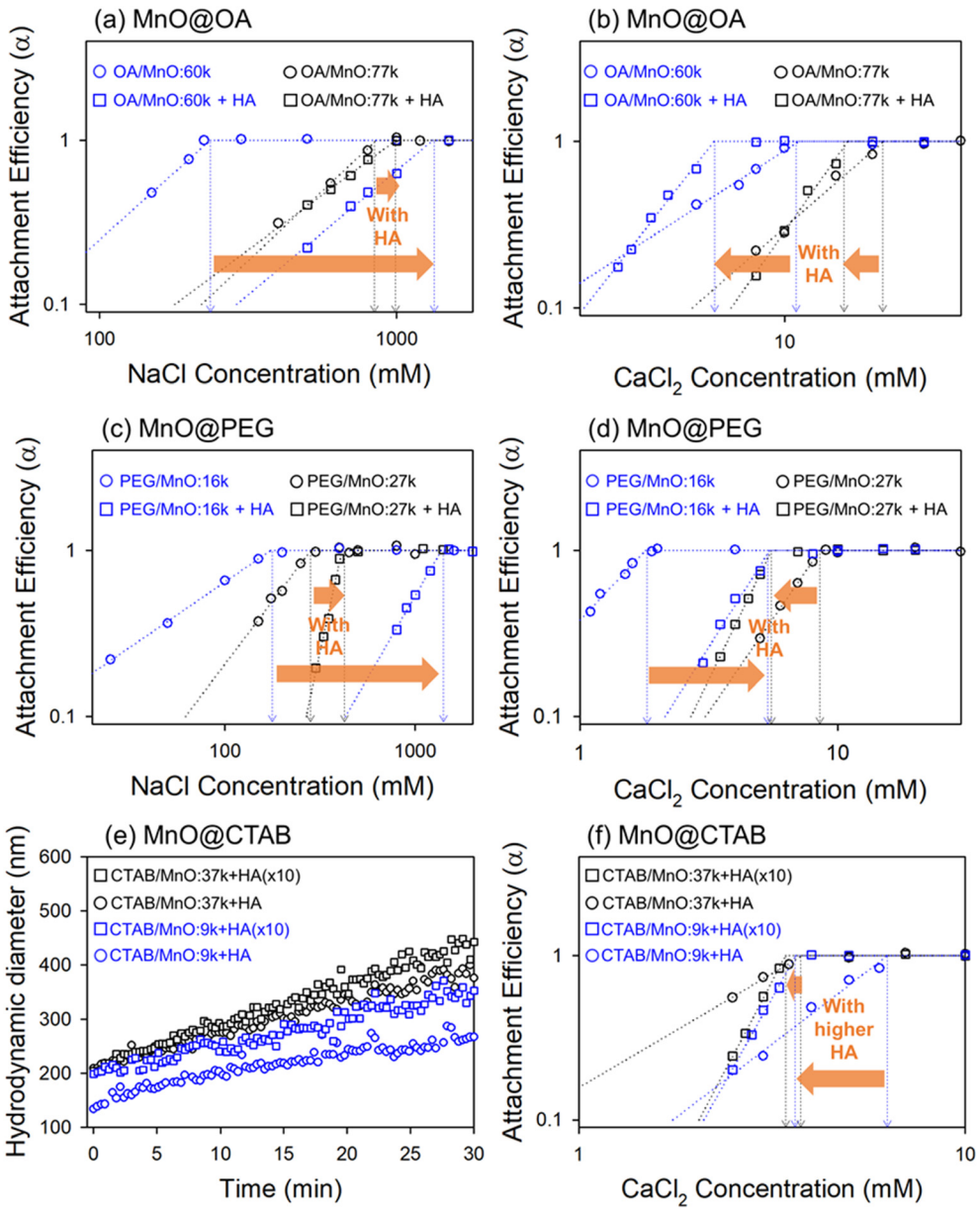

Fig. 2 Attachment efficiency (α) of organic coated Mn_xO_y NPs with different grafting densities (*e.g.* OA/MnO:60k refers to 60k molecules of OA per MnO of nanocrystals) as a function of NaCl and $CaCl_2$ concentrations in the absence and presence of humic acid (HA, 1 ppm) at pH 7.0 ± 0.2; (a and b) Mn_xO_y@OA, (c and d) Mn_xO_y@PEG, and (f) Mn_xO_y@CTAB. (e) Aggregation profiles of Mn_xO_y@CTAB NPs with different grafting densities in the presence of humic acid (HA) under 2 M of NaCl concentration.

colloidal stability of NPs once attached to their surface(s).[40,41] Our results show that the effect of HA on the stability of NPs is varied a function of grafting density. We hypothesize that HA can more readily attach to NPs with lower grafting density and effectively improve their stability due to possible (increased) hydrophobic interactions.[42] While the CCC values increased with HA as a function of NaCl concentration, HA actually enhanced aggregation in the presence of calcium (Ca^{2+}) through what is likely to be intermolecular bridging as shown by others,[40] resulting in lower CCC values (5.75 and 5.45 mM of $CaCl_2$ for Mn_xO_y@OA and Mn_xO_y@PEG, respectively). In addition, the slopes of attachment efficiency curves in the presence of HA are steeper than those obtained in the absence of HA for all types of surface coating evaluated. This observation was attributed by the adsorption of HA to NPs which can enhance relatively aggregation kinetic sensitivity.[43]

In comparison to Mn_xO_y@OA and Mn_xO_y@PEG, positively charged NPs (Mn_xO_y@CTAB) with varied grafting density, showed different behavior with regard to colloidal stability, especially with divalent cationic salt ($CaCl_2$) and HA (Fig. 2(f)). The CCC of Mn_xO_y@CTAB for higher grafting density (3.7 mM) is lower than lower grafting density (6.3 mM) in $CaCl_2$ with 1 mg L^{-1} of HA. We expected positively charged functional groups could more readily associate with negatively charged HA due to

the electrostatic attraction, thus resulting in lower CCC in $CaCl_2$. We verified that the D_H of higher grafting density (129 nm) was larger than lower grafting density (94.8 nm) in the presence of HA, indicating more HA adsorbed on Mn_xO_y@CTAB with higher grafting density. For a higher concentration of HA (10 mg L^{-1} TOC), the CCC values of both higher and lower grafting densities were similar (3.4 and 3.6 mM of $CaCl_2$) as shown in Fig. 2(f). At such high concentration of HA, NPs are likely to be completely coated by HA regardless of grafting density, thus identical CCC values. Aggregation kinetics for Mn_xO_y@CTAB in 2000 mM of NaCl in the presence of HA is presented in Fig. 2(e). Here, the aggregation rate increased with increase of grafting density in the same concentration of HA, which are consistent with results obtained from aggregation kinetics as a function of $CaCl_2$.

Transport behavior in water saturated porous media

We performed column studies in a water-saturated porous medium to evaluate the transport behavior of Mn_xO_y NPs with different grafting densities. Breakthrough curves (BTCs) of effluent concentration normalized by the influent concentration (C/C_0) for Mn_xO_y NPs transport through water saturated columns are presented in Fig. 3. For comparison, representative BTCs for non-reactive (control) tracer were obtained, with C/C_0 reaching 1.0. In addition, tracer BTC shapes were consistent for all columns, with steep increase and decrease of C/C_0, indicating ideal equilibrium transport behavior.[30,44] In contrast to tracer transport, BTCs for organic coated Mn_xO_y NPs never reached C/C_0 = 1, indicative of favorable particle-collector interactions. NP breakthrough then showed gradually decreasing concentration after maximum relative concentration (C/C_0) in all types of surface stabilizers. This observation indicates that significant portion of the NPs were retained irreversibly in the column and the retained NPs were slowly released from the sand, which is likely due to secondary minimum interactions between NPs and sand.[45] To capture NP release behavior, measured BTCs were fit using the MFT method with a first-order detachment term. The tailing behavior observed in the experimental BTCs

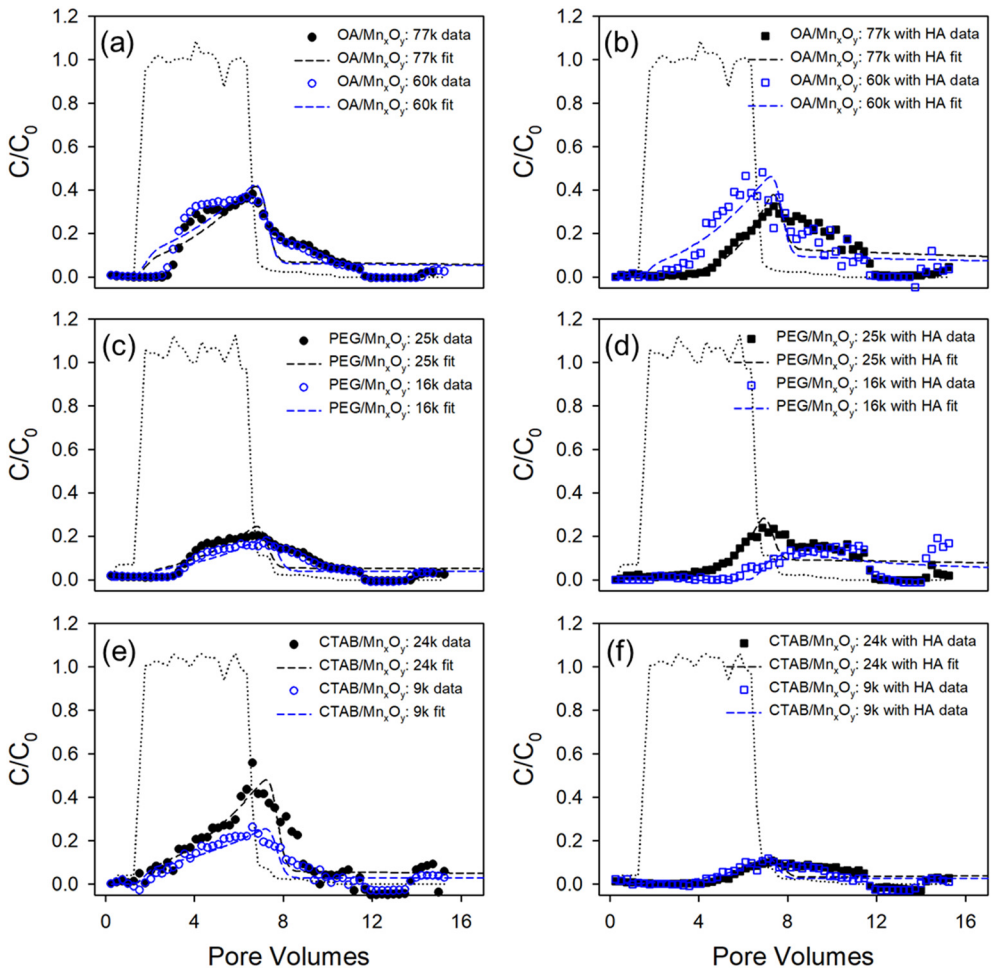

Fig. 3 Experimental and fitted breakthrough curves (BTCs) of Mn_xO_y NPs with different grafting densities in water saturated columns packed with 30–40 mesh Ottawa sand in the absence and presence of HA; (a and b) Mn_xO_y@OA, (c and d) Mn_xO_y@PEG, and (e and f) Mn_xO_y@CTAB. All column experiments were performed at 0.76 m d^{-1} of a pore-water velocity and pH 7.0 ± 0.2.

was successfully reproduced by the fitted curves. The fitted detachment rates for all investigated conditions were two orders of magnitude smaller than the attachment rates (Table S2†), indicating minimal NP release compared to attachment.

The C/C_0 of NPs with higher grafting density was similar or slightly higher than that of lower grafting density in the absence of HA. Whether the grafting density of the engineered NPs was high or low, all phase transferred NP samples were highly colloidally stable at the low electrolyte concentrations used in the column experiments (1 mM of KCl). In addition, the steric repulsion force for the bare sand could be lower than steric effects in aggregation of NPs, resulting in relatively less impact of grafting density on their deposition behavior. These results are similar to previous reports; the attachment efficiency of NPs to HA coated silica surface is lower than that of NPs to bare silica surface due to additional steric stabilization of HA on the silica surface.[41] Batch reactor experiments were also conducted as a function of grafting density of the engineered NPs to provide the supporting evidence regarding deposition behavior on sand (Table S1†). Similar or higher C/C_0 was achieved in higher grafting density and Mn_xO_y@CTAB showed highest C/C_0, followed by Mn_xO_y@OA and Mn_xO_y@PEG, which is consistent with their colloidal stabilities (and previously discussed results). The attachment efficiency (α) and single collector efficiency (η_0) of NPs to the sand calculated using eqn (2) and (3) are presented in Table 1. The resulting attachment efficiencies (α) were 0.0115 for Mn_xO_y@OA, 0.0227 for Mn_xO_y@PEG, and 0.0127 for Mn_xO_y@CTAB, respectively. The MFT fitted parameters (k_{att}, k_{det} and S_{max}) for three Mn_xO_y nanoparticles at two grafting density were also similar (Table S2†). For example, the fitted attachment rates for Mn_xO_y@OA, Mn_xO_y@PEG, and Mn_xO_y@CTAB were 1.20–1.38, 1.79–1.82, 1.43–1.46 h^{-1} at low and high grafting densities, respectively, indicating the surface coating density did not strongly influence the rate of NP attachment.

We observed negligible effects of HA on the C/C_0 for Mn_xO_y@OA and Mn_xO_y@PEG. Both negatively charged NPs likely have sufficient electrostatic repulsion forces, with respect to HA, for low electrolyte concentration. This is supported by identical D_H regardless of HA for Mn_xO_y@OA and Mn_xO_y@PEG as shown in Table 1. The MFT fitted S_{max} in the absence and presence of HA for Mn_xO_y@OA and Mn_xO_y@PEG were also similar (~1.5 μg g^{-1} sand), indicating the minimal effect of HA on the attachment of negatively charged Mn_xO_y. In comparison, for positively charged Mn_xO_y@CTAB, the C/C_0 significantly decreased in the presence of HA as also shown in Table 1 from 0.380 and 0.214 to 0.134 and 0.093 for higher and lower grafting densities, respectively. This result is consistent with the results of aggregation behavior in which HA adsorbs to the positively charged Mn_xO_y@CTAB and these larger aggregates were more likely to interact with a particle collector. We verified that the D_H of Mn_xO_y@CTAB NPs significantly increased with HA due to adsorption from 37.8 and 40.9 to 129 and 94.8 nm, respectively. Attachment efficiencies (α) of Mn_xO_y@CTAB to the soil media were also increased from 0.0127 and 0.0214 to 0.077 and 0.0647 for higher and lower grafting densities in the presence of HA, respectively (Table 1). The greater attachment in the presence of HA was also observed for MFT fitted k_{att} values, which increased from 1.43 h^{-1} to 3.2 h^{-1}. For all organic coatings, the BTCs shifted toward later time in presence of HA (the peak concentration arrival time was at higher pore volume). This change could be attributed to the change of transport properties in the soil column, as organic matter reduced NP transport.[46,47]

To determine the retention profile of NPs in soil media, we measured their concentrations in sectioned segments of column (Fig. S4†). As expected, the attached NPs were relatively more abundant in the first section of column (inlet) for all types of surface stabilizers, which is consistent with previous studies.[30,48] In the presence of HA, the highest retained concentration was observed in the second section of column for Mn_xO_y@OA and Mn_xO_y@PEG. We hypothesize that HA was substantially adsorbed to the first section of soil column and thus preventing negatively charged Mn_xO_y@OA and

Table 1 Single collector efficiency (η_0) and attachment efficiency (α) of Mn_xO_y NPs with different grafting density

Surface stabilizer	Grafting density	Hydrodynamic diameter (nm)	Single collector efficiency (η_0)	Relative concentration (C/C_0)	Attachment efficiency (α)
In the absence of HA					
OA	77k	27.8	0.36	0.33	0.012
	60k	25.1	0.39	0.33	0.010
PEG	25k	39.5	0.27	0.19	0.023
	16k	39.9	0.27	0.16	0.025
CTAB	24k	37.8	0.28	0.38	0.013
	9k	40.9	0.27	0.22	0.021
In the presence of HA					
OA	77k	28.7	0.35	0.30	0.013
	60k	29.2	0.36	0.36	0.011
PEG	25k	38.2	0.28	0.28	0.017
	16k	37.8	0.28	0.28	0.017
CTAB	24k	129	0.11	0.13	0.070
	9k	94.8	0.14	0.09	0.065

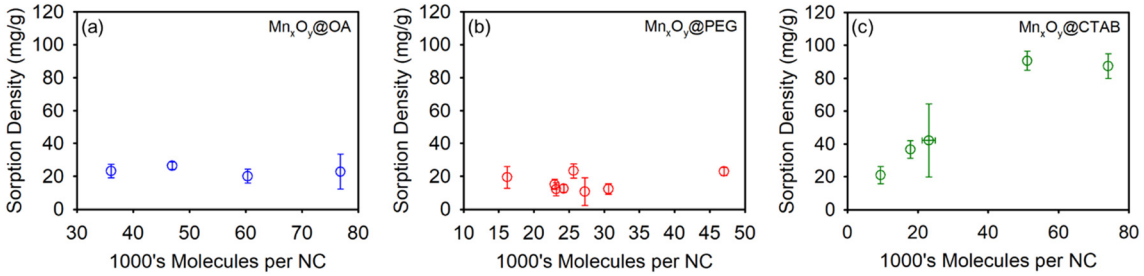

Fig. 4 Sorption density of organic coated Mn_xO_y NPs as a function of grafting density (1000's molecules per NC) for different surface coatings; (a) Mn_xO_y@OA, (b) Mn_xO_y@PEG, and (c) Mn_xO_y@CTAB. Every test was conducted in the presence of 10 mg L^{-1} of Cr(VI) at pH 7.0 ± 0.2.

Mn_xO_y@PEG from attaching to the sand. For Mn_xO_y@CTAB, however, retention of NPs was highest near the inlet and declined along the column, for which positively charged NPs could attach to the HA occupied on the collector surface.

Enhanced sorption with higher grafting density

Finally, we evaluated chromate sorption performance of Mn_xO_y NPs with various grafting densities for different surface stabilizers (OA, PEG, and CTAB). Positively charged Mn_xO_y@CTAB showed enhanced chromate sorption performance compared to negatively charged Mn_xO_y@OA and Mn_xO_y@PEG as observed previously by our group and others (Fig. 4).[16,49] Further, for Mn_xO_y@CTAB, higher grafting density resulted in higher Cr(VI) sorption density as shown in Fig. 4(c). The sorption density was 21, 37, 42, 90, and 87 mg g^{-1} (milligram of Cr per gram of NPs) for 9k, 18k, 24k, 51k, and 74k of grafting densities, respectively. As the dominant species of Cr(VI) at pH 7 is negatively charged $HCrO_4^-$ and CrO_4^{2-}, such correlation between Cr(VI) sorption density and grafting density of NPs is attributed to the increased number of favorable functional groups, thus simply providing more adsorbing sites. The maximum sorption observed at 51k and above, indicates steric hindrance plays a role at high(er) loadings. For negatively charged NPs (Mn_xO_y@OA and Mn_xO_y@PEG), while increasing grafting density plays critical role for colloidal stability, as discussed above, it does not provide additional (direct) sorption sites for negatively charged species. Sorption densities of Mn_xO_y@OA NPs were 23, 26, 20, and 23 mg g^{-1} for 36k, 47k, 60k, and 77k of grafting density, and Mn_xO_y@PEG NPs were 19, 15, 12, 12, 23, 11, 12, and 23 mg g^{-1} for 16k, 23k, 23k, 24k, 26k, 27k, 31k, and 47k of grafting density, respectively.

Conclusions

In this work, we describe the effects of grafting density on the colloidal stability, transport, and sorption behavior of the engineered Mn_xO_y NPs in water. Higher grafting densities lead to improved colloidal stability due to increasing steric repulsion forces. The stability of NPs was also dependent on HA with respect to grafting density. CCC (stability) values of negatively charged NPs with lower grafting density significantly increased in the presence of HA, while having negligible effects for NPs with higher grafting density. For positively charged NPs, more HA associates with higher grafting densities due to enhanced electrostatic attraction, resulting in decreasing CCC values, which is likely due to the intermolecular bridging in the presence of $CaCl_2$. Transport behavior was consistent with aggregation behavior regardless of grafting density for negatively charged Mn_xO_y@OA and Mn_xO_y@PEG, whereas positively charged Mn_xO_y@CTAB had increased deposition in the presence of HA. In addition, higher grafting density for Mn_xO_y@CTAB led to higher chromate sorption capacities, as additional (favorable) functional groups provided more sorption sites. Taken together this work clearly highlights the need for more precise NP synthesis protocols, including surface modification, which allow for critical comparison(s) of fundamental behavior. As demonstrated here, NP deposition and sorption behavior can strongly depend on surface density of stabilizing layers – a fact that remains under appreciated in many direct (nano)particle comparison studies done in an environmental context.

Conflicts of interest

There are no conflicts to declare.

Acknowledgements

This work is supported by U.S. Army Corps of Engineers (W912HZ-13-2-0009-P00001), the U.S. National Science Foundation (CBET 1437820), and U.S. Department of Agriculture, National Institute of Food and Agriculture (2018-67021-28319). XRD measurements were made possible by a grant from the U.S. National Science Foundation (EAR-1161543). TEM, DLS, ultracentrifugation, and ICP-OES were provided by the Nano Research Facility (NRF) at Washington University in St. Louis.

References

1 S. Kango, S. Kalia, A. Celli, J. Njuguna, Y. Habibi and R. Kumar, Surface modification of inorganic nanoparticles for development of organic–inorganic nanocomposites—a review, *Prog. Polym. Sci.*, 2013, **38**, 1232–1261.
2 R. A. Sperling and W. J. Parak, Surface modification, functionalization and bioconjugation of colloidal inorganic nanoparticles, *Philos. Trans. R. Soc., A*, 2010, **368**, 1333–1383.

3 M. A. Boles, D. Ling, T. Hyeon and D. V. Talapin, The surface science of nanocrystals, *Nat. Mater.*, 2016, **15**, 141.
4 D. Guo, G. Xie and J. Luo, Mechanical properties of nanoparticles: basics and applications, *J. Phys. D: Appl. Phys.*, 2013, **47**, 013001.
5 R. P. Bagwe, L. R. Hilliard and W. Tan, Surface modification of silica nanoparticles to reduce aggregation and nonspecific binding, *Langmuir*, 2006, **22**, 4357–4362.
6 C. Levard, E. M. Hotze, G. V. Lowry and G. E. Brown Jr, Environmental transformations of silver nanoparticles: impact on stability and toxicity, *Environ. Sci. Technol.*, 2012, **46**, 6900–6914.
7 Y. Li, W. Zhang, J. Niu and Y. Chen, Surface-coating-dependent dissolution, aggregation, and reactive oxygen species (ROS) generation of silver nanoparticles under different irradiation conditions, *Environ. Sci. Technol.*, 2013, **47**, 10293–10301.
8 W. Yantasee, C. L. Warner, T. Sangvanich, R. S. Addleman, T. G. Carter, R. J. Wiacek, G. E. Fryxell, C. Timchalk and M. G. Warner, Removal of heavy metals from aqueous systems with thiol functionalized superparamagnetic nanoparticles, *Environ. Sci. Technol.*, 2007, **41**, 5114–5119.
9 X. Zhao, W. Liu, Z. Cai, B. Han, T. Qian and D. Zhao, An overview of preparation and applications of stabilized zero-valent iron nanoparticles for soil and groundwater remediation, *Water Res.*, 2016, **100**, 245–266.
10 M. Shen, H. Cai, X. Wang, X. Cao, K. Li, S. H. Wang, R. Guo, L. Zheng, G. Zhang and X. Shi, Facile one-pot preparation, surface functionalization, and toxicity assay of APTS-coated iron oxide nanoparticles, *Nanotechnology*, 2012, **23**, 105601.
11 F. He and D. Zhao, Manipulating the size and dispersibility of zerovalent iron nanoparticles by use of carboxymethyl cellulose stabilizers, *Environ. Sci. Technol.*, 2007, **41**, 6216–6221.
12 T. Phenrat, N. Saleh, K. Sirk, H.-J. Kim, R. D. Tilton and G. V. Lowry, Stabilization of aqueous nanoscale zerovalent iron dispersions by anionic polyelectrolytes: adsorbed anionic polyelectrolyte layer properties and their effect on aggregation and sedimentation, *J. Nanopart. Res.*, 2008, **10**, 795–814.
13 X. Li, J. J. Lenhart and H. W. Walker, Aggregation kinetics and dissolution of coated silver nanoparticles, *Langmuir*, 2011, **28**, 1095–1104.
14 E. M. Hotze, T. Phenrat and G. V. Lowry, Nanoparticle aggregation: challenges to understanding transport and reactivity in the environment, *J. Environ. Qual.*, 2010, **39**, 1909–1924.
15 S. S. Lee, W. Li, C. Kim, M. Cho, B. J. Lafferty and J. D. Fortner, Surface functionalized manganese ferrite nanocrystals for enhanced uranium sorption and separation in water, *J. Mater. Chem. A*, 2015, **3**, 21930–21939.
16 C. Kim, S. S. Lee, B. J. Lafferty, D. E. Giammar and J. D. Fortner, Engineered superparamagnetic nanomaterials for arsenic (V) and chromium (VI) sorption and separation: quantifying the role of organic surface coatings, *Environ. Sci.: Nano*, 2018, **5**, 556–563.
17 Y. Huang and A. A. Keller, EDTA functionalized magnetic nanoparticle sorbents for cadmium and lead contaminated water treatment, *Water Res.*, 2015, **80**, 159–168.
18 D. Selli, S. Motta and C. Di Valentin, Impact of surface curvature, grafting density and solvent type on the PEGylation of titanium dioxide nanoparticles, *J. Colloid Interface Sci.*, 2019, **555**, 519–531.
19 J. Lin, H. Zhang, V. Morovati and R. Dargazany, PEGylation on mixed monolayer gold nanoparticles: Effect of grafting density, chain length, and surface curvature, *J. Colloid Interface Sci.*, 2017, **504**, 325–333.
20 D. N. Benoit, H. Zhu, M. H. Lilierose, R. A. Verm, N. Ali, A. N. Morrison, J. D. Fortner, C. Avendano and V. L. Colvin, Measuring the grafting density of nanoparticles in solution by analytical ultracentrifugation and total organic carbon analysis, *Anal. Chem.*, 2012, **84**, 9238–9245.
21 C. Kim and J. D. Fortner, Surface-Engineered Nanomaterials in Water: Understanding Critical Dynamics of Soft Organic Coatings and Relative Aggregation Density, *Environ. Sci. Technol.*, 2020, **54**, 13548–13555.
22 K. An, M. Park, J. H. Yu, H. B. Na, N. Lee, J. Park, S. H. Choi, I. C. Song, W. K. Moon and T. Hyeon, Synthesis of uniformly sized manganese oxide nanocrystals with various sizes and shapes and characterization of their T1 magnetic resonance relaxivity, *Eur. J. Inorg. Chem.*, 2012, **2012**, 2148–2155.
23 S. S. Lee, W. Li, C. Kim, M. Cho, J. G. Catalano, B. J. Lafferty, P. Decuzzi and J. D. Fortner, Engineered manganese oxide nanocrystals for enhanced uranyl sorption and separation, *Environ. Sci.: Nano*, 2015, **2**, 500–508.
24 K. L. Chen and M. Elimelech, Aggregation and deposition kinetics of fullerene (C60) nanoparticles, *Langmuir*, 2006, **22**, 10994–11001.
25 K. L. Chen, B. A. Smith, W. P. Ball and D. H. Fairbrother, Assessing the colloidal properties of engineered nanoparticles in water: case studies from fullerene C60 nanoparticles and carbon nanotubes, *Environ. Chem.*, 2010, **7**, 10–27.
26 R. C. Heath, *Basic ground-water hydrology*, US Geological Survey, 1983.
27 G. Grisak, W. Merritt and D. Williams, A fluoride borehole dilution apparatus for groundwater velocity measurements, *Can. Geotech. J.*, 1977, **14**, 554–561.
28 B. M. Patterson, M. D. Annable, E. B. Bekele and A. J. Furness, On-line groundwater velocity probe: Laboratory testing and field evaluation, *J. Contam. Hydrol.*, 2010, **117**, 109–118.
29 K.-M. Yao, M. T. Habibian and C. R. O'Melia, Water and waste water filtration. Concepts and applications, *Environ. Sci. Technol.*, 1971, **5**, 1105–1112.
30 Y. Li, Y. Wang, K. D. Pennell and L. M. Abriola, Investigation of the transport and deposition of fullerene (C60) nanoparticles in quartz sands under varying flow conditions, *Environ. Sci. Technol.*, 2008, **42**, 7174–7180.
31 N. Tufenkji and M. Elimelech, Correlation equation for predicting single-collector efficiency in physicochemical filtration in saturated porous media, *Environ. Sci. Technol.*, 2004, **38**, 529–536.

32 Y. Wang, M. D. Becker, V. L. Colvin, L. M. Abriola and K. D. Pennell, Influence of residual polymer on nanoparticle deposition in porous media, *Environ. Sci. Technol.*, 2014, **48**, 10664–10671.
33 G. Fritz, V. Schädler, N. Willenbacher and N. J. Wagner, Electrosteric stabilization of colloidal dispersions, *Langmuir*, 2002, **18**, 6381–6390.
34 C. Kim, S. S. Lee, K. T. Kwan, J. Lee, W. Li, B. J. Lafferty, D. E. Giammar and J. D. Fortner, Surface functionalized nanoscale metal oxides for arsenic(v), chromium(vi), and uranium(vi) sorption: considering single- and multi-sorbate dynamics, *Environ. Sci.: Nano*, 2020, **7**, 3805–3813.
35 C. Kim, J. Lee, D. Schmucker and J. D. Fortner, Highly stable superparamagnetic iron oxide nanoparticles as functional draw solutes for osmotically driven water transport, *npj Clean Water*, 2020, **3**, 8.
36 A. Prakash, H. Zhu, C. J. Jones, D. N. Benoit, A. Z. Ellsworth, E. L. Bryant and V. L. Colvin, Bilayers as phase transfer agents for nanocrystals prepared in nonpolar solvents, *ACS Nano*, 2009, **3**, 2139–2146.
37 A. J. Worthen, V. Tran, K. A. Cornell, T. M. Truskett and K. P. Johnston, Steric stabilization of nanoparticles with grafted low molecular weight ligands in highly concentrated brines including divalent ions, *Soft Matter*, 2016, **12**, 2025–2039.
38 B. Vincent, J. Edwards, S. Emmett and A. Jones, Depletion flocculation in dispersions of sterically-stabilised particles ("soft spheres"), *Colloids Surf.*, 1986, **18**, 261–281.
39 B. Peng, Z. Liu and Y. Jiang, Aggregation of DNA-grafted nanoparticles in water: The critical role of sequence-dependent conformation of DNA coating, *J. Phys. Chem. B*, 2022, **126**, 847–857.
40 K. L. Chen and M. Elimelech, Influence of humic acid on the aggregation kinetics of fullerene (C60) nanoparticles in monovalent and divalent electrolyte solutions, *J. Colloid Interface Sci.*, 2007, **309**, 126–134.
41 K. L. Chen and M. Elimelech, Interaction of fullerene (C60) nanoparticles with humic acid and alginate coated silica surfaces: measurements, mechanisms, and environmental implications, *Environ. Sci. Technol.*, 2008, **42**, 7607–7614.
42 B. Peng, P. Liao and Y. Jiang, Preferential interactions of surface-bound engineered single stranded DNA with highly aromatic natural organic matter: Mechanistic insights and implications for optimizing practical aquatic applications, *Water Res.*, 2022, **223**, 119015.
43 M. Elimelech, J. Gregory and X. Jia, *Particle deposition and aggregation: measurement, modelling and simulation*, Butterworth-Heinemann, 2013.
44 Y. Wang, Y. Li, J. D. Fortner, J. B. Hughes, L. M. Abriola and K. D. Pennell, Transport and retention of nanoscale C60 aggregates in water-saturated porous media, *Environ. Sci. Technol.*, 2008, **42**, 3588–3594.
45 Y. Tian, B. Gao, C. Silvera-Batista and K. J. Ziegler, Transport of engineered nanoparticles in saturated porous media, *J. Nanopart. Res.*, 2010, **12**, 2371–2380.
46 H. Liu, D. M. Forsmann, C. Kjærgaard, H. Saki and B. Lennartz, Solute transport properties of fen peat differing in organic matter content, *J. Environ. Qual.*, 2017, **46**, 1106–1113.
47 M. Larsbo, J. Koestel, T. Kätterer and N. Jarvis, Preferential transport in macropores is reduced by soil organic carbon, *Vadose Zone J.*, 2016, **15**, 1–7.
48 Y. Han, G. Hwang, D. Kim, S. A. Bradford, B. Lee, I. Eom, P. J. Kim, S. Q. Choi and H. Kim, Transport, retention, and long-term release behavior of ZnO nanoparticle aggregates in saturated quartz sand: Role of solution pH and biofilm coating, *Water Res.*, 2016, **90**, 247–257.
49 M. Kumari, C. U. Pittman Jr and D. Mohan, Heavy metals [chromium (VI) and lead (II)] removal from water using mesoporous magnetite (Fe3O4) nanospheres, *J. Colloid Interface Sci.*, 2015, **442**, 120–132.